

# Design and Characterization of an Aerosol Test Chamber for Emergency Response Patient Contamination Control Simulation and Research

Megan L. Steele<sup>1</sup>, Emily M. Spatz<sup>2</sup>, George P. Lemmer<sup>2</sup>, Jacob M. Denney<sup>2</sup>, Jeremy M. Slagley<sup>2</sup>, Casey W. Cooper<sup>2</sup>, Robert M. Eninger<sup>3</sup>

<sup>1</sup>Fenic, Ltd., Dayton, USA

<sup>2</sup>Department of Systems Engineering and Management, Air Force Institute of Technology, Wright-Patterson Air Force Base, Montgomery County, USA

<sup>3</sup>Air Force Materiel Command, Office of the Command Surgeon, Wright-Patterson Air Force Base, Montgomery County, USA  
Email: fenicLtd@gmail.com

**How to cite this paper:** Steele, M.L., Spatz, E.M., Lemmer, G.P., Denney, J.M., Slagley, J.M., Cooper, C.W. and Eninger, R.M. (2023) Design and Characterization of an Aerosol Test Chamber for Emergency Response Patient Contamination Control Simulation and Research. *Occupational Diseases and Environmental Medicine*, 11, 78-96.

<https://doi.org/10.4236/odem.2023.111005>

**Received:** December 27, 2022

**Accepted:** February 24, 2023

**Published:** February 27, 2023

Copyright © 2023 by author(s) and Scientific Research Publishing Inc.

This work is licensed under the Creative Commons Attribution International License (CC BY 4.0).

<http://creativecommons.org/licenses/by/4.0/>



Open Access

---

## Abstract

Contaminated or infected patients present a risk of cross-contamination for emergency responders, attending medical personnel and medical facilities as they enter a treatment facility. The controlled conditions of an aerosol test chamber are required to examine factors of contamination, decontamination, and cross-contamination. This study presents the design, construction, and a method for characterizing an aerosol test chamber for a full-sized manikin on a standard North Atlantic Treaty Organization litter. The methodology combined air velocity measurements, aerosol particle counts and size distributions, and computational fluid dynamics modeling to describe the chamber's performance in three dimensions. This detailed characterization facilitates future experimental design by predicting chamber performance for a variety of patient-focused research.

## Keywords

Test Chamber Characterization, Aerosol Generation, Exposure Chamber Design, Air Velocity Mapping, Spatial Variability, CFD Modeling, Patient Decontamination

---

## 1. Introduction

The COVID-19 pandemic has brought bioaerosols and their transmission to the

forefront of the medical community's minds, as the risk of infection among medical providers and support staff remains high. Massive efforts were made early in the pandemic to control infection via decontamination and control of infected patients' excreta. Now that the disease has become endemic throughout the world and a large portion of the population has developed some immunity either naturally (via infection), from vaccination, or both, there is still an interest in decontamination research. New variants of the virus emerge through natural mutation in the face of immune response. Care facilities have modified how they provide care during operations [1] [2], during transportation [3] [4], and during routine care [5]. The medical community was able to adapt quickly in part due to lessons learned from the spread of other dangerous airborne pathogens and in part due to the rapid response of the scientific community in establishing key features of transmission and bioaerosol decontamination.

Much of past research in patient decontamination practices resulted in recommendations for removing or inactivating chemical, biological, or radiological agents without serious damage to the patient or medical personnel. Chilcott *et al.* [6] reported on the mass testing of United States government planned patient decontamination protocols on 86 volunteer subjects using surrogate agents. A key concern is not only reducing risk to the patient, but also reducing risk to attending medical personnel. If medics are contaminated by in-coming patients, they may spread that contamination, and also possibly suffer the effects of that agent. Infectious patients may act as a biological source and spread the agent as an aerosol via breathing, coughing, and sneezing. Schilling *et al.* [7] summarized methods for patient contamination control during short and long-distance transport in Europe. Given the lack of quantitative studies supporting patient decontamination strategies, Titus *et al.* [8] recommend focused studies to evaluate the efficacy of different decontamination methods. An aerosol test chamber large enough to place a full-size manikin would be useful to experiment on varying patient decontamination methods to inform medical facility design.

Flow-thru aerosol chambers for evaluating bioaerosol samplers and other collection devices have been used for several decades [9] [10] [11] [12]. Su *et al.* [9] investigated two novel bioaerosol samplers using a small wind tunnel. Experiments were conducted in air speeds between  $0.5 \text{ m}\cdot\text{s}^{-1}$  to  $2.0 \text{ m}\cdot\text{s}^{-1}$  in the  $0.76 \times 0.76 \times 1.4 \text{ m}$  test chamber. Upton *et al.* [10] tested three bioaerosol samplers in an  $8 \times 0.6 \times 1.2 \text{ m}$  wind tunnel at wind speeds ranging from  $0.4$  to  $4 \text{ m}\cdot\text{s}^{-1}$ . King *et al.* [11] estimated the size distributions of culturable particles and organisms using an Andersen bioaerosol impactor with real-time particle size distribution validated with an aerodynamic particle sizer (APS). In order to characterize the size distribution of impacted particles and organisms, a 200 mm diameter duct was used to transport the test bioaerosol to the Andersen impactor. This well mixed duct allowed for periodic real-time sampling through a side port connected to an APS inlet. The system was finely controlled via a fan with digital flow meter. But these three chambers were not large enough for full-scale human or manikin decontamination studies. Emanuel *et al.* [12] detected and tracked

biological simulant particles through reaerosolization and an outdoor release event. During indoor reaerosolization tests, *Bacillus thuringiensis* subsp. *kurstaki* test particles were lofted in a 61 m long chamber using fans that produced a  $3.8 \text{ m}\cdot\text{s}^{-1}$  breeze. This chamber was certainly large enough for full-scale research, but has limited availability.

These studies provide robust characterization of samplers for measuring bioaerosols but the ability to confirm bioaerosol presence and concentration are only a portion of patient decontamination studies. In addition to detection, patient decontamination studies require patient analogs and medical equipment to allow for a real representation of bioaerosol behavior in a medical setting. There is a dearth of studies focused solely on patient decontamination in controlled environments. To address this short-coming researchers in this study designed, fabricated, and characterized an aerosol chamber capable of fitting a North Atlantic Treaty Organization (NATO) standard patient litter and full body manikin. The chamber was designed to be cost-effective, modular and capable of generating air velocities representative of a variety of workplaces. The current study adds to the existing chambers and increases the availability of characterized research facilities. While studies in other aerosol chambers of sufficient size did not focus on patient decontamination, they did underscore the importance of thorough chamber characterization. Temperature, pressure, and relative humidity can all have substantial effects on aerosol characteristics so researchers must decide from the outset if the chamber should be designed to control these parameters or if it is sufficient to simply monitor them [13] [14] [15] [16] [17]. Studies cannot begin without a complete understanding of the chamber characteristics, to include the achievable air velocities, airflow patterns, spatial and temporal variability of particle movement, and air exchange rates and mixing behavior of the chamber [14] [15] [16] [18] [19]. For the aerosol chamber described in this paper, temperature, pressure and relative humidity were monitored and all air velocities corrected for variations.

Aerosol test chambers are commonly characterized in conjunction with computational fluid dynamics (CFD) techniques to verify and validate models and code [20] [21] [22] [23]. When considering any fluid flow, the fundamental set of equations used to describe the conservation of momentum and mass transport are the Navier-Stokes equations, specifically in regard to incompressible turbulent flows [24]. While it is true that air is compressible, the Navier-Stokes equations are routinely used to describe airflow [25]. Given that the chamber will support a myriad of studies with different equipment, manikins, and obstacles to airflow, researchers created computational fluid dynamic simulations of the unoccupied chamber. These simulations, in combination with the chamber's ability to accommodate both patient analogs and bioaerosol generation, make it a unique asset among decontamination studies. The remainder of this paper describes the chamber's design and characterization; including air velocity in three dimensions, aerosol concentration and size distribution, and the

computational fluid dynamics model developed to describe the airflow.

## 2. Objective and Research Question

The chamber design focused on two research projects: measurement of airflows and aerosol transport around a litter-bound patient, and decontamination of the same litter-bound patient. These patients and the medical staff attending them would be expected to experience environments as varied as outdoors, medical treatment areas, and aeromedical evacuation on military aircraft. As these projects had varied requirements and future needs are unknown, design of the chamber was meant to maximize flexibility by modularity of design. Due to the size of a standard NATO litter (0.584 m (1.9 ft) wide) and space available at the research facility, researchers decided that 0.762 m by 0.762 m (2.5 ft × 2.5 ft) would be the minimum cross-section considered to avoid boundary effects [26]. Air velocities inside the chamber needed to be similar to those encountered in common indoor workplaces, from treatment room spaces which approach calm environments ( $<0.3 \text{ m}\cdot\text{s}^{-1}$ ) to those spaces which require robust ventilation to protect against particulate hazards ( $\geq 0.5 \text{ m}\cdot\text{s}^{-1}$ ) [27] [28]. Considering the desire to mimic these environments, researchers determined that ambient air conditions would be suitable and no effort was made to control temperature or humidity.

Early designs aimed for laminar flow inside the chamber and basic fluid dynamics calculations were undertaken to determine if this would be possible within the space constraints. A range of air temperatures, air velocities, and chamber cross-sections were considered although ultimately, it was determined to be impossible to achieve laminar or fully developed turbulent flow.

As calculations indicated that achieving laminar and fully developed turbulent flow would be impossible within the real-world space constraints, the final design was a rectangular chamber with dimensions of  $0.914 \times 0.914 \times 6.401$  meters ( $3 \times 3 \times 21$  feet). Polycarbonate was chosen as the material for the walls, to allow researchers to monitor experiments. Though the chamber was designed to operate under negative pressure, a 0.762 cm (0.3 in) wall thickness was deemed adequate as the magnitude of the pressure would be small. The frame was constructed out of aluminum (80/20 Inc., Columbia City, IN). The final chamber design and fabrication was in three 2.13 m (7 ft) sections which could be joined at the seams to form a single continuous chamber (Figure 1). The middle section included a door to allow access to the interior of the chamber. Air enters and is exhausted through banks of high efficiency particulate air (HEPA) filters. Air is moved through the chamber by a centrifugal fan equipped with a variable frequency drive located downstream (Model HDBI-120, Cincinnati Fans, Cincinnati, OH).

After construction, all inside seams were caulked to seal them and the seams between chamber sections were sealed with Gorilla Tape<sup>®</sup> (Gorilla Glue, Inc., Cincinnati, OH) to facilitate detachment for cleaning or relocation. Once these activities were completed, characterization of the chamber began.

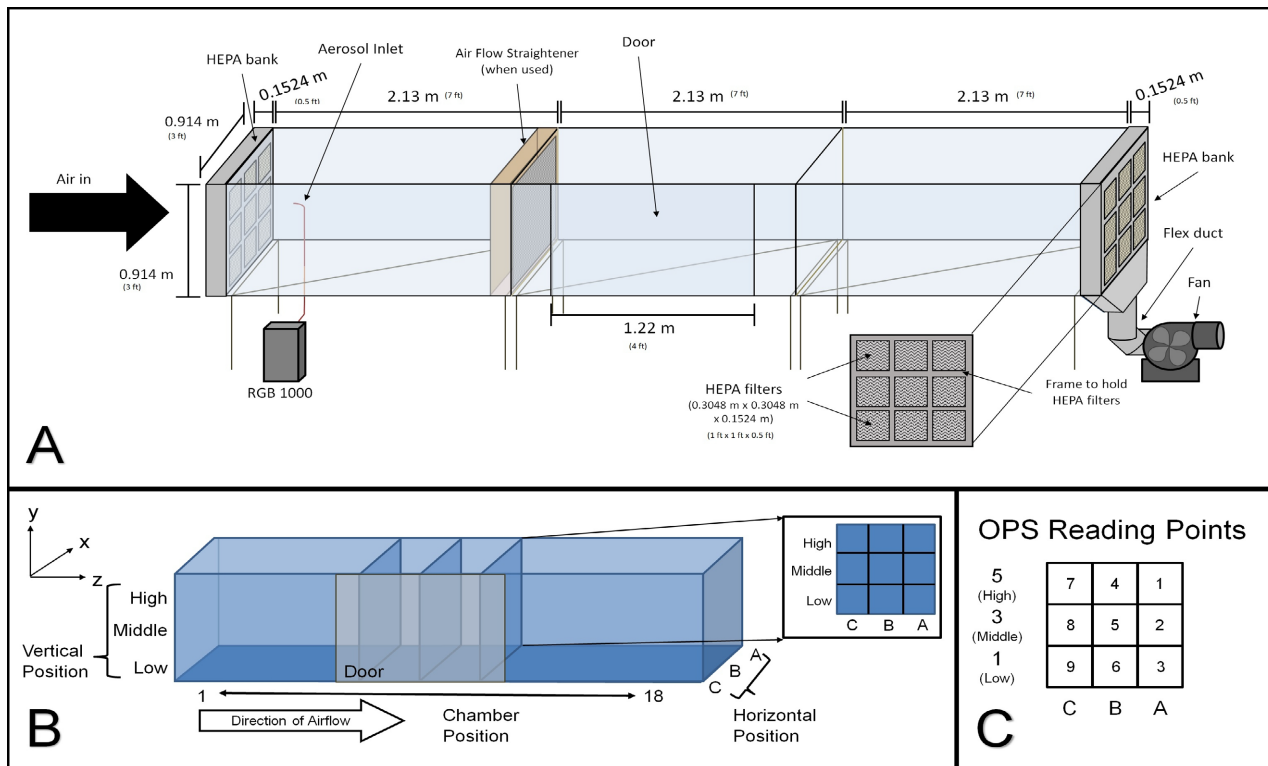


**Figure 1.** Final Chamber Design. (A) Final chamber design with dimensions. (B) Simplified chamber design showing measurement locations. (C) Optical particle sizer measurement positions in a cross-sectional plane.

As turbulence was expected, some characterization was conducted with a flow straightener (Model: AS100, Ruskin, Kansas City, MO) in place. It was located just upstream of the door, at the seam between the first and middle chambers. All tests without the flow straightener included measurements from all three chambers, while those with the flow straightener only measured locations downstream of the flow straightener placement.

### 3. Methodology

The chamber had to be characterized for both air velocities and aerosol particle counts to facilitate the design of experiments for patient contamination control research.

#### 3.1. Velocity Mapping

Velocity mapping was done to understand the air speed characteristics along the face of each plane and longitudinally along the length of the chamber. Mapping was done using a VelGrid attached to an AirData Multimeter data logger (Model: ADM-880c, Shortridge Instruments, Inc., Scottsdale, AZ).

The VelGrid is designed to measure the face velocity profile by covering a  $0.356 \times 0.356 \text{ m}^2$  area and recording the average velocity from 16 points within this area. In this experiment, three VelGrids were stacked and used simultaneously to cover a vertical slice of a plane in the chamber. Data were recorded using the ADM-880c in automatic mode, which were downloaded from the de-

vice at regular intervals. The ADM-880c has the capability to automatically correct measured velocities for atmospheric temperature and pressure variations, although it cannot account for fluctuation in relative humidity. This was done manually by using the air temperature and relative humidity collected by a Kestrel 4000 Pocket Weather Tracker (KestrelMeter.com, Boothwyn, PA) which was set to record data every 20 minutes.

To measure the velocity in the aerosol chamber, it was divided into imaginary blocks of  $0.305\text{ m} \times 0.305\text{ m} \times 0.305\text{ m}$  (1 ft  $\times$  1 ft  $\times$  1 ft). Starting in chamber 1, the chamber was labelled in 0.305-meter (1-foot) increments along the z-axis (**Figure 2**). The chamber was lettered along the x-axis, with the cube on the side of the chamber furthest from the door being labelled “A”, the middle labelled “B”, and the one nearest the door labelled “C”. In addition, each VelGrid was given a number, used to designate the height it measured within the chamber, although the words “high”, “middle”, and “low” are used for clarity.

In the initial measurement of air velocity, the three VelGrids were stacked by attachment to a ring stand. The face of the VelGrids was positioned at each measurement location in the chamber, using tape marks on the chamber to ensure alignment. Once the VelGrids were positioned, the ADM-880c data loggers were attached and turned on to begin recording data. The chamber door was closed, the two side seams were sealed with tape, and the fan was turned on.

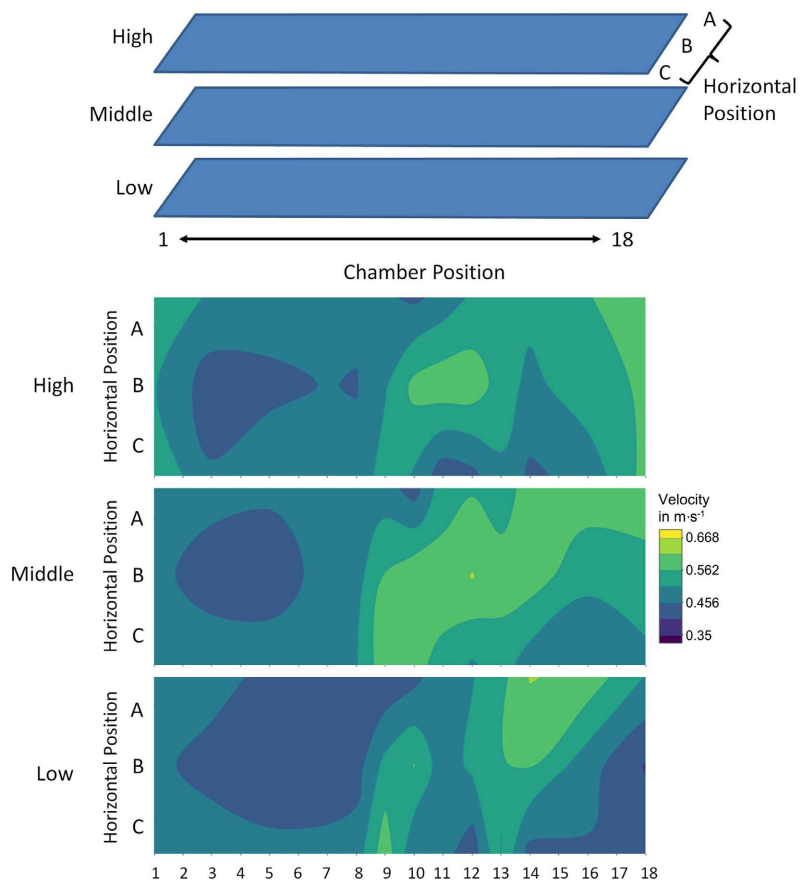


**Figure 2.** Horizontal velocity profiles in the chamber at  $0.5\text{ m}\cdot\text{s}^{-1}$ , no flow straightener.

For each run, the fan was dialed up through the desired speeds using the variable frequency drive. In order to characterize the velocity across the full range of the fan, three frequencies were chosen: 16 Hz, 30 Hz, and 60 Hz. It was determined that 60 Hz would provide an air speed of  $1 \text{ m}\cdot\text{s}^{-1}$ , 30 Hz would provide  $0.5 \text{ m}\cdot\text{s}^{-1}$ , and 16 Hz would provide  $0.2 \text{ m}\cdot\text{s}^{-1}$ . From this point on, the fan settings will be referred to by the speed, rather than the frequency. The lower end was chosen to be slightly above the limit of detection of the ADM-880c data logger ( $0.127 \text{ m}\cdot\text{s}^{-1}$ ). For each run, the fan was dialed to  $0.2 \text{ m}\cdot\text{s}^{-1}$  and allowed to stabilize for a minute before a three-minute measurement period began. After the measurement period, the fan was dialed to  $0.5 \text{ m}\cdot\text{s}^{-1}$ , given a minute to stabilize and then measured for three minutes. Finally, the fan was dialed to  $1 \text{ m}\cdot\text{s}^{-1}$  and the stabilization and measurement periods were repeated. Once measurements were complete, the fan was turned off, the chamber opened, and the VelGrids were moved to the next measurement location along the x-axis. For the initial set of data, measurement locations were done sequentially (1A, 1B, 1C, 3A, 3B, 3C, etc.).

To validate the repeatability of measurements, certain locations within the chamber were selected for duplicate measurements on different days. One third of the original sampling locations were sampled for repeatability (14 of 39 without the flow straightener, and 9 of 27 with the flow straightener in place).

In addition to the initial air speed characterization, the air velocities were measured while clean air ran through a dust generator to ensure that the introduction of another air stream for aerosol research did not significantly disrupt the established airflow patterns. Sampling planes were chosen based on those planes with the most consistent air velocities. Two planes were chosen for use when the flow straightener was not present (5 and 7) and two planes which could be used when the flow straightener was in place (8 and 10). These measurements were repeated with two different settings on the dust generator, a high (250 kPa) and low (100 kPa) pressure-induced flow, to ensure that the full operational range of the dust generator could be used without significant effect on the established airflow patterns. Final analysis showed no impact to the established patterns so aerosol studies commenced.

### **3.2. Spatial Variability of Aerosol Particle Count Concentration**

Spatial variability of the chamber was examined using UltraFine Arizona Road Dust (ARD) (Particle Technology Inc., Arden Hills, MN) lofted by a rotating brush generator (RBG) 1000 dust generator (Palas GMBH, Karlsruhe, Germany) while real-time measurements were obtained with a particle counter. Measurements were taken in the same planes as were sampled with clean air (5 and 7 without the flow straightener, and 8 and 10 with the flow straightener in place).

Sampling probes channeled dust from the chamber to an optical particle sizer, OPS model 3330 (TSI, Inc., Shoreview, MN) to obtain particle size distribution and particle count concentration information. One OPS reading was taken for

two minutes, then the probe was moved to a new location. The end of the sampling probe was positioned in the center of each grid square. Sampling was not isokinetic as the opening of the probe was perpendicular to airflow, though any errors due to this would be equivalent for each location.

For initial tests, the fan was set to  $0.5 \text{ m}\cdot\text{s}^{-1}$ . After the fan was turned on, the RBG dust generator was turned on. The compressed air line was set to 552 kPa, and the pressure regulator on the RBG was set to 100 kPa. The feed rate was set to 60 mm/hr. This gave a run time of approximately 40 minutes in most cases based on the amount of the dust reservoir filled. The brush speed was set to 1200 revolutions per minute per the manufacturer recommendation. Fifteen samples were taken per plane and experiments repeated on multiple days to capture inter-day variability.

#### 4. Computational Fluid Dynamics Model Development

This study used COMSOL Multiphysics<sup>®</sup> (version 5.4), a multiphysics solver which uses a finite element method [29]. The model was a standard  $k$ - $\epsilon$  turbulence method with steady state conditions considering gravity. To account for hydrostatic pressure, a two-equation model using Reynolds Averaged Navier-Stokes (RANS) and wall functions was used. This model is recommended for use with high Reynolds numbers and low Mach numbers indicating incompressible flow, which is representative of the exposure chamber flow conditions [29]. The Reynolds number range for this model was 4265 to 59,468. The standard  $k$ - $\epsilon$  model is robust and commonly used to model airflow around bluff bodies, which is an important consideration for future work.

The aerosol chamber design was imported to COMSOL software from a 3-dimensional computer-aided design (CAD) file that allowed for an accurate digital representation of the chamber as the computational domain. The model was created full size and used the HEPA filter bank as the inlets, one for each filter, with additional inlets at the door to account for improper seals. An 11-inlet model was designed which accounted for leaks in the door as recorded with hot wire anemometer described below. This model was deemed to be the best representative model of the exposure chamber based on the velocity profile obtained during characterization.

The model considered each of the nine HEPA filters as an inlet boundary condition with the velocity determined by measuring face velocity at the filter exterior with a hot wire anemometer. During the process of model development, the best results applied a 10% increase to the observed face velocity measurement. An additional two inlets were included at the bottom of the door to represent leaks. The outlet boundary condition was constant pressure set at the location of the plane at the exhaust outlet. The initial conditions were set by the experimentally determined conditions at plane 1 with pressure set to 98.4 kPa, temperature set to 294 K and velocity of  $0.51 \text{ m}\cdot\text{s}^{-1}$  (representative of average chamber velocity).

The governing equations are the RANS equations with transport equations for  $k$  and  $\varepsilon$  shown (Equations (1) and (2)). The experimental conditions reflected steady temperature as there were no heat sources or sinks within the exposure chamber. Gravity was considered to account for hydrostatic pressure and larger particle settling for applicability to future experiment. The geometry for the exposure chamber was created using CAD software with the design specifications and post-construction measurements. The mesh was left in free tetrahedral form generated by the software algorithm but had a finer mesh along the walls due to concerns with element size compared to the corners and inlet geometries. The mesh would need to be refined for future work that included more complex geometries inside the chamber but was adequate for validation of velocity profiles at each chamber location. The mesh consisted of 1,262,836 elements with 1,040,112 tetrahedral, 11,418 pyramid, and 211,306 prism elements. **Table 1** lists the variables.

**Table 1.** Nomenclature for Equations (1) and (2).

Definitions of Variables		
Variable	Definition	Equation or Value
$\mu_T$	Turbulent Viscosity	$\mu_T = \rho * C_\mu \left( \frac{k^2}{\varepsilon} \right)$
$\rho$	Fluid Density—depends on temperature, pressure, and fluid	Constant for incompressible flow
$C_\mu$	Constant	0.09
$k$	Turbulent Kinetic Energy	Equation (1)
$\varepsilon$	Turbulent Dissipation Rate	Equation (2)
$u$	Velocity Field	User Input
$\nabla$	Gradient/Partial Differential	
$\mu$	Fluid Dynamic Viscosity—relates the shear stress and shear rates of a liquid	
$\sigma_k$	Constant	1.0
$P_k$	Production Term	$P_k = \mu_T \left( \nabla u : (\nabla u + (\nabla u)^T) - \frac{2}{3} (\nabla \cdot u)^2 \right) - \frac{2}{3} \rho k \nabla \cdot u$
$T$	Temperature – user-defined reference temperature or calculated from other model inputs	
$\sigma_\varepsilon$	Constant	1.3
$C_{\varepsilon 1}$	Constant	1.44
$C_{\varepsilon 2}$	Constant	1.92
$B$	Surface roughness (Constant or user-defined)	5.2
$\kappa_v$	von Kármán constant	0.41

The measured velocity profile was compared to numerical simulation by averaging the computed solutions across the face of the imaginary blocks (*i.e.* 1A-low, with nine blocks per plane). The velocity field solutions were exported from COMSOL Multiphysics<sup>®</sup> and sorted, filtered, and averaged using Python (version 3.7.1, Jupyter Notebook version 5.7.4) to return the velocity profile average for each block. When comparing measured and simulated values, a total of 117 squares were considered from the characterization. The comparison was made based on the confidence interval (C.I.) of measurements from the ADM-880c. Locations that were measured multiple times were considered highly variable if repeated measurements fell outside the C.I. of the original measurement and thus were not considered ideal for model verification and validation. Locations where repeated measurements all fell within the respective C.I.s were considered good locations for validation and weighted more heavily in analysis. Locations that were only measured once were considered based on the C.I. of the single measurement.

Of 117 squares, nine were considered highly variable based on the criteria (7.7%). There were a remaining 54 squares (46.2%) with multiple measurements and 54 (46.2%) with only a single measurement. For model validation purposes, if the simulated value fell within the observed range with C.I., it was considered a valid simulated value with less emphasis given to highly variable locations due to the larger inclusion range.

Equation (1). Definition of  $k$

$$\rho(\partial k/\partial t) + \rho u \cdot \nabla k = \nabla \cdot ((\mu + \mu_T/\sigma_k)\nabla k) + P_k - \rho \varepsilon. \quad (1)$$

Equation (2). Definition of  $\varepsilon$

$$\rho(\partial \varepsilon/\partial t) + \rho u \cdot \nabla \varepsilon = \nabla \cdot ((\mu + \mu_T/\sigma_\varepsilon)\nabla \varepsilon) + C_{\varepsilon 1}(\varepsilon/k)P_k - C_{\varepsilon 2}\rho(\varepsilon^2/k). \quad (2)$$

## 5. Results and Analysis

### 5.1. Chamber Air Velocity and Aerosol Measurement Results

Velocity data were visualized as contour plots using the open source software R (Version 3.6.0). Breakpoints for the velocity were chosen based on the VelGrid's precision,  $\pm 3\%$  or  $\pm 0.04 \text{ m}\cdot\text{s}^{-1}$  ( $\pm 3\%$  or  $\pm 7 \text{ fpm}$ ) [30]. When plotted, data for the entire chamber without a flow straightener showed unevenness of flow throughout the chamber, though the least variability was observed in the middle slice of the chamber, away from horizontal position C. All three fan speeds showed velocity extremes at chamber locations 9 and 12, indicating gaps in the door even with taping the door seams.

Considering the uneven profiles collected along the chamber length, measurements were taken across different days to verify the repeatability of measurements. In **Figure 3**, the initial measurements are shown as black dots. Measurements collected on subsequent days are shown as red and blue dots. The pink ribbon shows the uncertainty surrounding the initial measurements. The Grubbs' test was used to determine any data points that were outliers ( $\alpha = 0.05$ ).

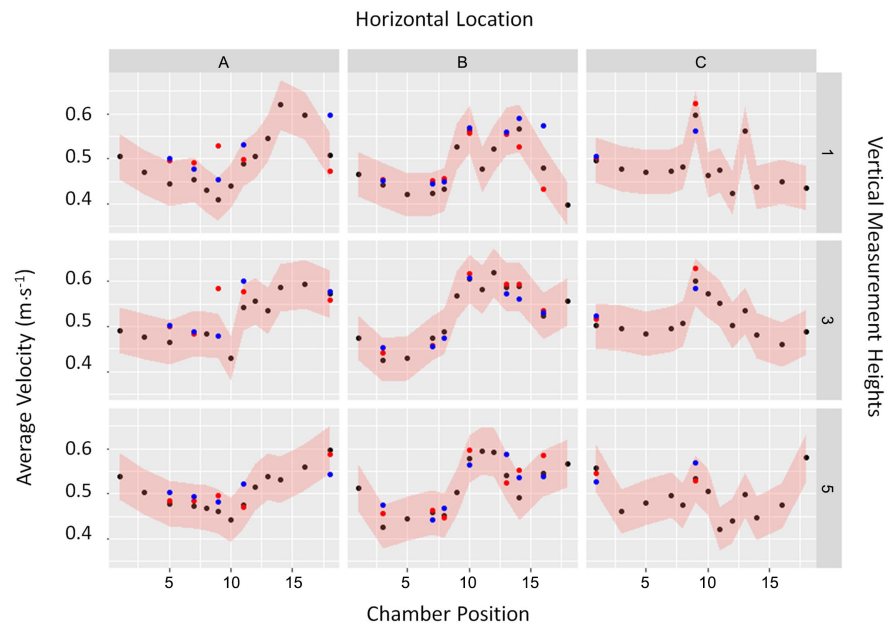


**Figure 3.** Day-to-day variability in average velocity at  $0.5 \text{ m}\cdot\text{s}^{-1}$ , no flow straightener. Black dots indicate the first day's measurement, red and blue dots indicate the second and third subsequent days' measurements.

The only outliers found were in the  $0.2 \text{ m}\cdot\text{s}^{-1}$  data. Results were similar for velocities measured with the flow straightener. The variability observed was deemed controlled enough to proceed with further characterization without modification of the chamber.

Velocity data were evaluated qualitatively and quantitatively for normality using quantile-quantile plots and the Shapiro-Wilk test. Data collected without a flow straightener did not behave normally; however, those collected with the flow straightener in place did behave normally.

Due to non-normality, the data were tested for equal variance using Levene's test and a significance of 0.05 was chosen as the cutoff. Data were tested for a variety of conditions: the longitudinal chamber position alone, the chamber position with regard to the vertical position, the chamber position with regard to the horizontal position, and the horizontal position with regard to the vertical position. Of these conditions, it was desirable to achieve either equal variance along the chamber length or equal variance within one plane at a specific chamber position. With respect to only the chamber position, equal variance could not be assumed for fan speeds  $0.5$  and  $1 \text{ m}\cdot\text{s}^{-1}$ . The null hypothesis could not be rejected for any fan speed when considering the horizontal and vertical position, suggesting that in a plane at a specific chamber location, equal variance exists. While equal variance for chamber position with respect to the vertical or horizontal positions failed to reject the null, these conditions were not physically meaningful as they implied a long rectangular prism with equal variance, but unequal velocities. It is unlikely any research scenario would rely on that specific combination of conditions.

These results for the horizontal and vertical position interaction were qualita-

tively evaluated through boxplots. The conclusion remains the same though the extent of the variances is visually more apparent.

Owing to the unfavorable velocity profiles in the second chamber, planes 5 and 7 were chosen for further characterization. Ultrafine Arizona Road Dust was lofted and OPC readings were taken at nine points within each plane. Every two-minute sample at a single location in the plane was transformed from raw counts to the mass mean aerodynamic diameter through the process described by Hinds [31]. The only difference between the calculations presented by Hinds [31] was the mass of the dust,  $500 \text{ kg/m}^3$ . The MMAD calculated from each reading was plotted by horizontal position, then vertical position to discern if the aerosol distribution was more stable from side-to-side or top-to-bottom in the plane (Figure 4). The  $0.5 \text{ m}\cdot\text{s}^{-1}$  setting yielded the most consistent results though the MMAD reported at any fan setting and any location only ranged from  $3.5 - 4.25 \mu\text{m}$ . The average MMAD observed was  $3.9 \mu\text{m}$  (GSD  $1.82 \mu\text{m}$ ), while the manufacturer reported an MMAD of  $4.32 \mu\text{m}$ . While the observed particle size distribution was slightly smaller than that reported by the manufacturer, the GSD indicates a narrowly dispersed aerosol. As isokinetic sampling was not conducted, the discrepancy in median diameters may be explained by fewer of the large particles making it into the sampling probe, which was held perpendicular to the freestream. As well, the MMAD ( $3.4 - 4.9 \mu\text{m}$ ) and GSD ( $1.5 - 2.1 \mu\text{m}$ ) did not differ substantially between planes or runs, suggesting that for the ultrafine particles that even dispersion was achieved.

All data gathered and analyzed confirmed initial design expectations, in the flow was turbulent and irregular along any plane of interest. Aerosol distribution data were encouraging as the distribution, if not the raw counts, were similar at all nine points sampled for each plane. Given this discovery along with the positioning of the aerosol inlet, the aerosols were considered well mixed in the chamber. Considering the MMAD boxplots, contours of the velocity and particle count profiles were generated to visualize airflow and aerosol patterns by plane (Figure 5). These final contours served as guidelines for follow-on research sampler placement.

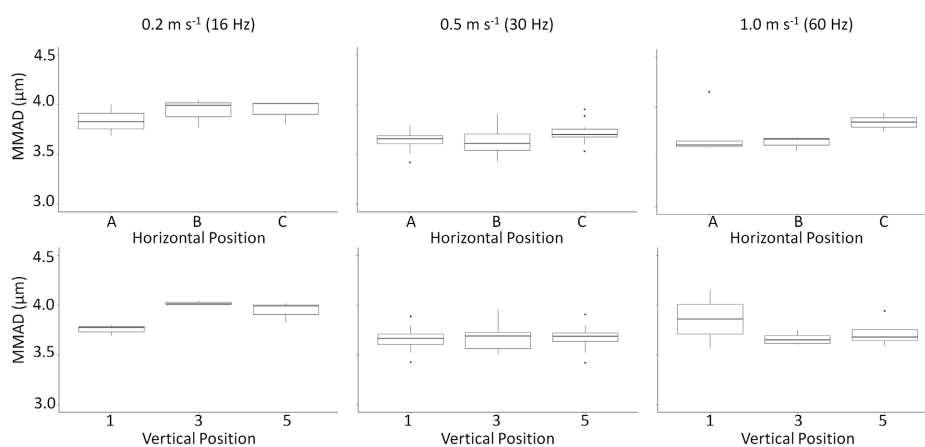
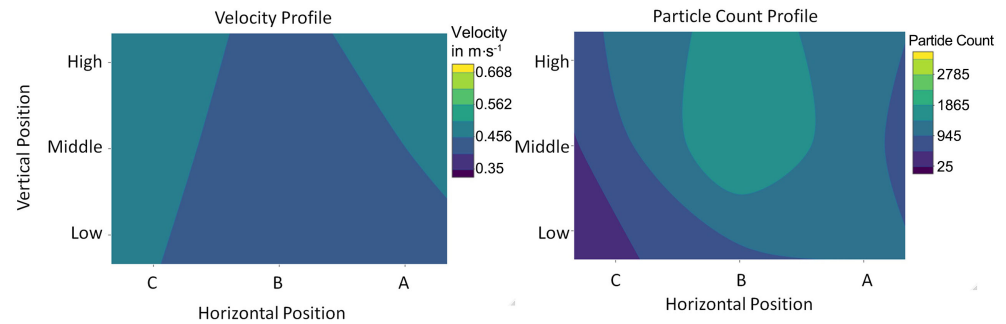


Figure 4. MMAD boxplots for plane 5.



**Figure 5.** Velocity and particle count profiles in plane 5 at  $0.5 \text{ m}\cdot\text{s}^{-1}$ .

International Organization for Standardization (ISO) 14644-3 standard, *Cleanroom and Associated Controlled Environments—Part 3: Test Methods*, recommends a test of time for the room to achieve a 100-fold reduction in test aerosol concentration [32]. It should be noted that the test is specified for non-unidirectional airflow rooms or zones. A clean room is characterized and certified for performance periodically.

The chamber described in this study was not designed as a clean room, although there are many common concepts. There are HEPA filters on the inlet and the exhaust of the chamber so that only particles intentionally introduced for experiments are present. Also, the exhaust filter ensures that particles do not escape into the ambient background air in the larger room. The chamber is a uni-directional airflow room. The chamber was characterized as described in this paper, and chamber procedures were recorded in a standard operating procedure. The standard operating procedure for the chamber requires real-time monitoring of the particle concentration and not opening the chamber until the concentration returns to background levels. The characterization trials used an optical particle counter and polystyrene latex (PSL) spheres of  $1 \mu\text{m}$  diameter. PSL spheres were introduced up to a raw count of 300,000 particles. When the particle generator was turned off, the particle count dropped back to background within 2 minutes. This was done repeatedly. When considering variability in experimental procedures, it was determined that approximately 40 air changes was sufficient, which results in a mandatory 10 minute wait with the chamber exhaust fan running to reduce particle concentrations to background. The real-time instrument also serves as a check on particle reduction. If a specific experiment results in longer decay time, then the experimental protocol can be modified immediately to ensure that particle concentrations decay to background. This differs from a clean room approach with periodic certification. Once the experiment ceased and particles were exhausted, then a standardized research protocol dictated how to handle any waste, such as simulated patient decontamination trash. For instance, researchers donned gloves and respirators, opened the access door, wiped down and removed equipment or samples and double-bagged any biological materials for later autoclave and disposal.

While obtaining additional measurements for the CFD model, it was discovered that an unidentified leak at the door was allowing air to infiltrate the space.

After creating a new seal to address this gap, additional measurements of select planes in chambers 2 and 3 were collected to determine the impact on their flow profile. As seen in **Figure 6**, previously disordered plane 9 showed marked improvement in flow, to the point where the second chamber velocity profiles indicated it could reliably be used for experiments. This effectively doubled the volume of sampling space with minimum structural alterations. Unfortunately, the third chamber remained highly disordered, likely owing to effects from proximity to the fan.

## 5.2. CFD Model Results

The simulation results fell within measurement confidence intervals as observed in experiments for 90/117 (76.92%) squares overall and 47/54 (87.04%) of the squares with multiple measurements. Four of the forty-five locations shown had model values which fell outside of the measurement C.I.s. Five of the nine highly variable locations occurred in either plane 9 or 10, indicating the door leak was impacting consistent measurements in those locations. The model reasonably simulated the characterization based on the velocity profile at each plane (**Figure 7**).

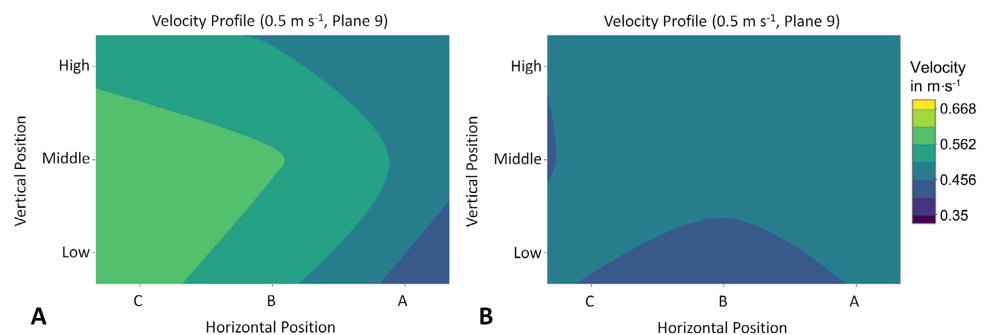


**Figure 6.** Velocity profile comparison for plane 9 at  $0.5 \text{ m}\cdot\text{s}^{-1}$  (A) original door seal and (B) improved door seal.

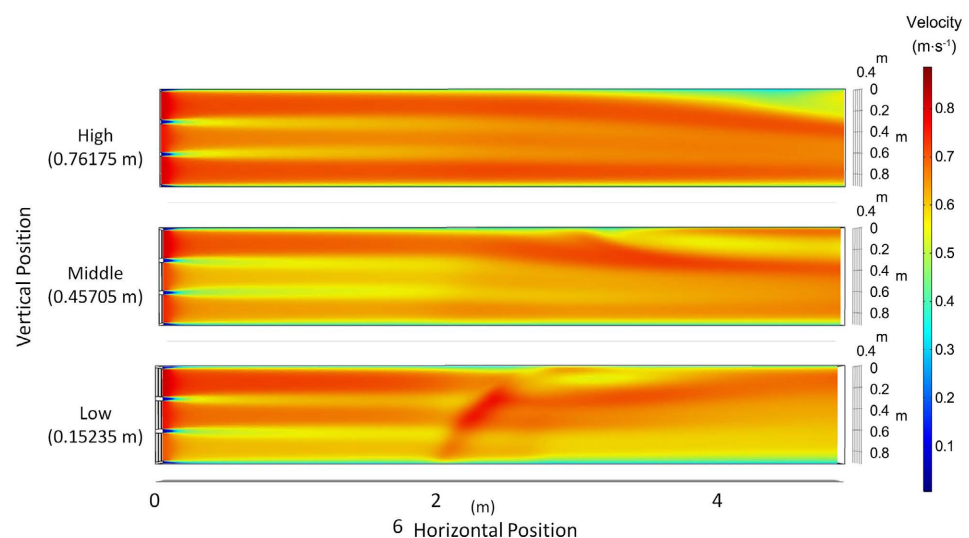


**Figure 7.** Airflow visualization from CFD model.

In contrast to figures showing measured values, simulated values are only from a slice at the precise height indicated. The metal frame which holds the HEPA filters in place prevents airflow, shown by the slow-moving airflow at the inlet for each plane in **Figure 7**.

The mesh was left in the free tetrahedral form generated by the software algorithm but had a finer mesh along the walls due to concerns with element size compared to the corners and inlet geometries. The mesh would need to be refined for future work that included more complex geometries inside the chamber but was adequate for validation of velocity profiles at each chamber location.

## 6. Conclusions and Recommendations

A 6.401 m (21 ft) chamber with 0.835 m<sup>2</sup> (9 ft<sup>2</sup>) cross-section was constructed to serve as a test space for aerosol studies investigating patient contamination control. This study demonstrated a method for the rigorous characterization of a flow through aerosol chamber. The combination of aerosol size distribution, air velocity profiles, and computational fluid dynamics model facilitate a wide range of research experiments. Aerosol sampler comparison studies have used this chamber's data to plan the location of the samplers to optimize their results [33] [34]. Personal decontamination studies have also used the chamber data for planning their experiments [35]. The chamber characterization reduced time spent on pilot studies for each experiment. Air flow profiles were generated by measuring velocity at prescribed locations along the x-, y-, and z-axes. Aerosol size distribution profiles were created for the four planes identified as most stable with and without the flow straightener. Inter-day variability was deemed acceptable considering the limitations of the anemometer. This finding supports the use of the chamber for future studies without modification. While equal variance existed across x-y planes in the chamber, the magnitude of the variance was considerable. This considerable variance suggests researchers must either collect large sample sets to detect significance among the data or restrict their activities to a smaller, better defined subsection of a given plane.

The creation of a computational fluid dynamics model validated by physical measurements will be a great asset to future research projects. It will allow researchers to predict the impact to flow behavior when different sampling apparatus are in place before conducting pilot research. It is apparent that improvements to the door's seal could be made and CFD models could inform an improved design as well as behavior after modification. Finally, the air flow was only characterized at three fan settings, and aerosol behavior at a single fan speed. It stands to reason that subsequent research may rely on intermediate velocities to achieve their research aims. Refinement of the current model would allow predictions to be made of flow behavior that could easily be validated with judicious sampling, rather than a repeat of the entire characterization outlined in this report. This CFD model will ultimately help save researchers time and funds.

The data collected and analyzed in this study confirm the chamber performance is stable enough for a variety of research aims. Periodic confirmation of

chamber performance is recommended. Any significant changes to the setup, including replacement of the access door require a complete recharacterization. With the present setup, researchers will need to conduct pilot studies to capture any bias inherent in the selected chamber location before proceeding to full scale studies, though use of the CFD model will aid this process.

The chamber described in this paper is able to accommodate a patient litter, unlike the chambers described by Upton *et al.* [10], King and McFarland [11], and Su *et al.* [9]. The minimum air velocity achievable,  $0.2 \text{ m}\cdot\text{s}^{-1}$ , is more representative of a calm environment like those found indoors compared to those tested in the aforementioned studies, where the lowest velocity tested was  $0.4 \text{ m}\cdot\text{s}^{-1}$  [10]. None of the studies included CFD simulations. However, the chamber described by Su *et al.* [9] provided an additional length to introduce and mix aerosols prior to the experimental section and was capable of achieving air velocities up to  $2 \text{ m}\cdot\text{s}^{-1}$ . In a scenario where first responders are providing emergency services to a patient while outdoors, air velocities greater than  $1 \text{ m}\cdot\text{s}^{-1}$  may be recorded. The extended length of the chamber in Emanuel *et al.* [12] is ideal for reaerosolization studies and is 9.5 times the length available in this study's chamber. Given the cost and physical constraints of the location available for this chamber, only 6.4 m of internal space was available. For high air velocity situations, this may be insufficient to capture the furthest distances bioaerosols may be deposited after reaerosolization.

Future improvements for the chamber should include systems which control the air temperature and humidity to allow researchers to simulate specific environments of concern. While the current method of recording these parameters does allow data to be appropriately corrected, it limits researchers to ambient conditions. Similarly, the panels in the middle chamber should be replaced for a better seal around the door to prevent ambient air intrusion. While initial studies are focused in the first third of the chamber and are therefore less impacted by the air intrusion, future studies would benefit from a less turbulent environment at the door seal.

## Acknowledgements

This work was supported by the United States Air Force, 711 Human Performance Wing, Airman Systems Directorate, Warfighter and Medical Optimization Division, under Grant #2019-073, and Grant #FA8650-17-C-6834.

## Disclaimer

The views expressed in this article are those of the authors and do not reflect the official policy or position of the Air Force Institute of Technology, the United States Air Force, the Department of Defense, or the United States government.

## Conflicts of Interest

The authors declare no conflicts of interest regarding the publication of this paper.

## References

- [1] Dexter, F., Elhakim, M., Loftus, R.W., Seering, M.S. and Epstein, R.H. (2020) Strategies for Daily Operating Room Management of Ambulatory Surgery Centers Following Resolution of the Acute Phase of the COVID-19 Pandemic. *Journal of Clinical Anesthesia*, **64**, Article ID: 109854. <https://doi.org/10.1016/j.jclinane.2020.109854>
- [2] Ti, L.K., Ang, L.S., Foong, T.W. and Ng, B.S.W. (2020) What We Do When a COVID-19 Patient Needs an Operation: Operating Room Preparation and Guidance. *Canadian Journal of Anesthesia*, **67**, 756-758. <https://doi.org/10.1007/s12630-020-01617-4>
- [3] Osborn, L., Meyer, D., Dahm, P., Ferguson, B., Cabrera, R., Sanger, D., Mock, M., Herrera, T., Mader, S. and Ostrosky-Zeichner, L. (2020) Integration of Aeromedicine in the Response to the COVID-19 Pandemic. *JACEP Open*, **1**, 557-562. <https://doi.org/10.1002/emp2.12117>
- [4] Yousuf, B., Sujatha, K.S., Alfoudri, H. and Mansurov, V. (2020) Transport of Critically Ill COVID-19 Patients. *Intensive Care Medicine*, **46**, 1663-1664. <https://doi.org/10.1007/s00134-020-06115-1>
- [5] Krist, A.H., DeVoe, J.E., Cheng, A., Ehrlich, T. and Jones, S.M. (2020) Redesigning Primary Care to Address the COVID-19 Pandemic in the Midst of the Pandemic. *Annals of Family Medicine*, **18**, 349-354. <https://doi.org/10.1370/afm.2557>
- [6] Chilcott, R.P., Lerner, J., Durrant, A., Hughes, P., Mahalingam, D., Rivers, S. and Reppucci, J. (2019) Evaluation of US Federal Guidelines (Primary Response Incident Scene Management [PRISM]) for Mass Decontamination of Casualties during the Initial Operational Response to a Chemical Incident. *Annals of Emergency Medicine*, **73**, 671-684. <https://doi.org/10.1016/j.annemergmed.2018.06.042>
- [7] Schilling, S., Follin, P., Jarhall, B., Tegnell, A., Lastilla, M., Bannister, B. and Puro, V. (2009). European Concepts for the Domestic Transport of Highly Infectious Patients. *Clinical Microbiology and Infection*, **15**, 727-733. <https://doi.org/10.1111/j.1469-0691.2009.02871.x>
- [8] Titus, E., Lemmer, G., Slagley, J. and Eninger, R. (2019) A Review of CBRN Topics Related to Military and Civilian Patient Exposure and Decontamination. *American Journal of Disaster Medicine*, **14**, 137-149. <https://doi.org/10.5055/ajdm.2019.0324>
- [9] Su, W.C., Tolchinsky, A.D., Chen, B.T., Sigaev, V.I. and Cheng, Y.S. (2012) Evaluation of Physical Sampling Efficiency for Cyclone-Based Personal Bioaerosol Samplers in Moving Air Environments. *Journal of Environmental Monitoring*, **14**, 2430-2437. <https://doi.org/10.1039/c2em30299c>
- [10] Upton, S.L., Mark, D., Douglass, E.J., Hall, D.J. and Griffiths, W.D. (1994) A Wind Tunnel Evaluation of the Physical Sampling Efficiencies of Three Bioaerosol Samplers. *Journal of Aerosol Science*, **25**, 1493-1501. [https://doi.org/10.1016/0021-8502\(94\)90220-8](https://doi.org/10.1016/0021-8502(94)90220-8)
- [11] King, M.D., Thien, B.F., Tiirikainen, S. and McFarland, A.R. (2009) Collection Characteristics of a Batch-Type Wetted Wall Bioaerosol Sampling Cyclone. *Aerobiologia*, **25**, 239-247. <https://doi.org/10.1007/s10453-009-9129-3>
- [12] Emanuel, P.A., Buckley, P.E., Sutton, T.A., Edmonds, J.M., Bailey, A.M., Rivers, B.A. and Gibbons, H.S. (2012) Detection and Tracking of a Novel Genetically Tagged Biological Simulant in the Environment. *Applied and Environmental Microbiology*, **78**, 8281-8288. <https://doi.org/10.1128/AEM.02006-12>
- [13] Hagerman, I., Isaxon, C., Gudmundsson, A., Wierzbicka, A., Dierschke, K., Ber-

- glund, M., Pagels, J., Nielsen, J., Assarsson, E., Andersson, U.B.K., Xu, Y., Jonsson, B.A.G. and Bohgard, M. (2014) Effects on Heart Rate Variability by Artificially Generated Indoor Nano-Sized Particles in a Chamber Study. *Atmospheric Environment*, **88**, 165-171. <https://doi.org/10.1016/j.atmosenv.2014.02.003>
- [14] Isaxon, C., Dierschke, K., Pagels, J.H., Wierszbicka, A., Gudmundsson, A., Löndahl, J., Hagerman, I., Berglund, M., Assarsson, E., Andersson, U.B., Jonsson, B.A.G., Nojgaard, J.K., Eriksson, A., Nielsen, J. and Bohgard, M. (2013) Realistic Indoor Nano-Aerosols for a Human Exposure Facility. *Journal of Aerosol Science*, **60**, 55-66. <https://doi.org/10.1016/j.jaerosci.2013.02.003>
- [15] Lidén, C., Lundgren, L., Skare, L., Lidén, G., Tornling, G. and Krantz, S. (1998) A New Whole-Body Exposure Chamber for Human Skin and Lung Challenge Experiments—The Generation of Wheat Flour Aerosols. *Annals of Occupational Hygiene*, **42**, 541-547. [https://doi.org/10.1016/S0003-4878\(98\)00063-5](https://doi.org/10.1016/S0003-4878(98)00063-5)
- [16] Lundgren, L. (2006) Large Organic Aerosols in a Human Exposure Chamber: Applications in Occupational Dermatology and Lung Medicine. Doctoral Thesis, Karolinska Institutet, Solna. <http://hdl.handle.net/10616/39694>
- [17] Rønborg, S.M., Mosbech, H., Johnsen, C.R. and Poulsen, L.K. (1996) Exposure Chamber for Allergen Challenge: The Development and Validation of a New Concept. *Allergy: European Journal of Allergy and Clinical Immunology*, **51**, 82-88. <https://doi.org/10.1111/j.1398-9995.1996.tb04562.x>
- [18] Lundgren, L., Skare, L., Lidén, C. and Tornling, G. (2006) Large Organic Aerosols in a Dynamic and Continuous Whole-Body Exposure Chamber Tested on Humans and on a Heated Mannequin. *Annals of Occupational Hygiene*, **50**, 705-715.
- [19] Pieretti, L.F. and Hammad, Y.Y. (2018) Performance of a Whole-Body Human Dust Inhalation Challenge Exposure Chamber. *Toxicology Reports*, **5**, 793-799. <https://doi.org/10.1016/j.toxrep.2018.07.004>
- [20] Li, J., Yavuz, I., Celik, I. and Guffey, S. (2007) Predicting Worker Exposure—The Effect of Ventilation Velocity, Free-Stream Turbulence and Thermal Condition. *Journal of Occupational and Environmental Hygiene*, **4**, 864-874. <https://doi.org/10.1080/15459620701665688>
- [21] Lin, C.H., Dunn, K.H., Horstman, R.H., Topmiller, J.L., Ahlers, M.F., Bennett, J.S., Sedgwick, L.M. and Wirogo, S. (2005) Numerical Simulation of Airflow and Airborne Pathogen Transport in Aircraft Cabins—Part I: Numerical Simulation of the Flow Field. *ASHRAE Transactions*, **111**, 755-763.
- [22] Lucci, F., Castro, N.D., Rostami, A.A., Oldham, M.J., Hoeng, J., Pithawalla, Y.B. and Kuczaj, A.K. (2018) Characterization and Modeling of Aerosol Deposition in Vitrocell<sup>®</sup> Exposure Systems—Exposure Well Chamber Deposition Efficiency. *Journal of Aerosol Science*, **123**, 141-160. <https://doi.org/10.1016/j.jaerosci.2018.06.015>
- [23] Zhang, Y., Sun, Y., Wang, A., Topmiller, J.L. and Bennett, J.S. (2005) Experimental Characterization of Airflows in Aircraft Cabins, Part II: Results and Research Recommendations. *ASHRAE Transactions*, **111**, 53-59.
- [24] White, F.M. (2011) Fluid Mechanics. 7th Edition, McGraw-Hill, New York.
- [25] Lai, A.C. and Chen, F. (2006) Modeling Particle Deposition and Distribution in a Chamber with a Two-Equation Reynolds-Averaged Navier-Stokes Model. *Journal of Aerosol Science*, **37**, 1770-1780. <https://doi.org/10.1016/j.jaerosci.2006.06.008>
- [26] NATO (National Atlantic Treaty Organization) (2013) Stretchers, Bearing Brackets and Attachment Supports. NATO Standard AMedP-2.1.
- [27] Baldwin, P.E.J. and Maynard, A.D. (1998) A Survey of Wind Speeds in Indoor Workplaces. *Annals of Occupational Hygiene*, **42**, 303-313.

- [https://doi.org/10.1016/S0003-4878\(98\)00031-3](https://doi.org/10.1016/S0003-4878(98)00031-3)
- [28] Bennett, J., Marlow, D., Nourian, F., Breay, J., Feng, A. and Methner, M. (2018) Effect of Ventilation Velocity on Hexavalent Chromium and Isocyanate Exposures in Aircraft Paint Spraying. *Journal of Occupational and Environmental Hygiene*, **15**, 167-181. <https://doi.org/10.1080/15459624.2017.1401710>
- [29] Comsol, A.B. (2018) CFD Module User's Guide. COMSOL Multiphysics®. (Version 5.4). COMSOL AB, Stockholm. <https://doc.comsol.com/5.4/doc/com.comsol.help.cfd/CFDModuleUsersGuide.pdf>
- [30] Shortridge Instruments (2015) Airdata Multimeter ADM-880c Manual.
- [31] Hinds, W.C. (1999) *Aerosol Technology: Properties, Behavior, and Measurement of Airborne Particles*. 2nd Edition, John Wiley and Sons, Inc., Hoboken.
- [32] International Organization for Standardization (2019) *Cleanrooms and Associated Controlled Environments—Part 3: Test Methods (ISO Standard No. 14644-3: 2019)*. <https://www.iso.org/obp/ui/#iso:std:iso:14644:-3:ed-2:v2:en>
- [33] Steele, M.L. (2020) *Assessing Challenges Associated with Sampling Hexavalent Chromium under New Consensus Guidelines*. Theses and Dissertations, Air Force Institute of Technology, Wright-Patterson AFB, No. 3256. <https://scholar.afit.edu/etd/3256>
- [34] Ohms, S.A. (2020) *Development and Characterization of a Filter-Based Bioaerosol Sampler Capable of Integration into Small Unmanned Aerial Systems*. Theses and Dissertations, Air Force Institute of Technology, Wright-Patterson AFB, No. 3249. <https://scholar.afit.edu/etd/3249>
- [35] Chapman, J.M. (2021) *Re-Aerosolization of Dense Metal Oxide Simulating Radiological Contamination from Military Clothing*. Theses and Dissertations, Air Force Institute of Technology, Wright-Patterson AFB, No. 4940. <https://scholar.afit.edu/etd/4940>